VIVID: In Vivo End-to-End Molecular Communication Model for COVID-19

Saswati Pal, *Student Member, IEEE,* Nabiul Islam, *Member, IEEE*, and Sudip Misra, *Senior Member, IEEE*

Abstract—As an alternative to ongoing efforts for vaccine development, scientists are exploring novel approaches to provide innovative therapeutics, such as nanoparticle- and stem cell-based treatments. Thus, understanding the transmission and propagation dynamics of coronavirus inside the respiratory system has attracted researchers' attention. In this work, we model the transmission and propagation of coronavirus inside the respiratory tract, starting from the nasal area to alveoli using molecular communication theory. We performed experiments using COMSOL, a finite-element multiphysics simulation software, and Python-based simulations to analyze the end-to-end communication model in terms of path loss, delay, and gain. The analytical results show the correlation between the channel characteristics and pathophysiological properties of coronavirus. For the initial 50% of the maximum production rate of virus particles, the path loss increases more than 16 times than the remaining 50%. The delayed response of the immune system and increase in the absorption of virus particles inside the respiratory tract delay the arrival of virus particles at the alveoli. Furthermore, the results reveal that the virus load is more in case of asthmatic patients as compared to the normal subjects.

Index Terms—Coronavirus, covid-19, nanonetwork, molecular communication, channel modeling, transmission model, virus propagation.

I. INTRODUCTION

WORLD Health Organization (WHO) has declared the COVID-19, novel coronavirus disease, as a public health emergency. The COVID-19 has taken the form of a pandemic due to its severe contagiousness, with currently more than 95 million cases and more than 2 million fatalities globally [1]. The novel coronavirus (known as SARS-CoV-2/CoV-2[1]), which is related to the SARS-CoV family (Severe Acute Respiratory Syndrome), has the serious potential to cause an acute respiratory tract infection. Its core is a single-stranded zoonotic RNA genome encapsulated inside a lipid envelope. It causes several symptoms, including high fever, dry cough, and breathing difficulty. In particular, it is transmitted from one person to another through an infected person's respiratory droplets, direct contact, or aerosols containing CoV-2.

The current preventive strategies employed worldwide to treat the CoV-2 include travel restrictions, testing and tracing, and sterilizing surfaces, hampering the worldwide social and economic frameworks. Currently, global research has resulted

Saswati Pal is with School of Nano-Science and Technology, Indian Institute of Technology Kharagpur, India.

Nabiul Islam is with Telecommunications Software and Systems Group, Waterford Institute of Technology, Ireland.

Sudip Misra is with Department of Computer Science and Engineering, Indian Institute of Technology Kharagpur, India (e-mail: smisra@cse.iitkgp.ac.in).

[1]Henceforth, referred to as CoV-2, for simplicity.

in vaccine trials on animals to study the host immune response. Since CoV-2 envelopes a mutating RNA, it is more likely to escape the effect of vaccination. Thus, the developed vaccine might not be effective in treating the current CoV-2 strain [2]. Considering these aspects, one of the alternative strategies to effectively treat CoV-2 infection is utilizing mesenchymal stem cell therapy, or anti-cytokine therapy [3], [4]. The therapy prevents the activation of the cytokine storm in the host immune system, otherwise causing multi-organ infection. Such therapies require a detailed transmission model of CoV-2 to assist the treatment.

Molecular communication (MC) is an interdisciplinary, emerging communication paradigm that facilitates communication among entities, with sizes ranging from micro-scale to nano-scale, via molecules. Based on varied propagation distance covered by molecules, different MC systems and applications exist, such as gap junction-based (nm-μm), bacteria-based (μm-mm) [5], and pheromone-based (cm-m) [6]. In this paper, we propose utilizing MC techniques to identify and model the virus transmission dynamics in vivo.

CoV-2 is transmitted inside the human body mostly via the respiratory tract. However, the virus also enters through the gastro-intestinal tract. In this work, we focus on the transmission of CoV-2 via the respiratory tract. Our proposed work involves modeling the transmission and propagation of CoV-2 inside the respiratory tract once the virus particles get attached to the nasal passage. In particular, we focus on the virus amplification, propagation, and reception along the respiratory tract by taking into account the effect of diffusion and advection due to airflow. Moreover, we analyze the impact of the immune system in the growth as well as the propagation of CoV-2 through the channel. The following list constitutes the major research *contributions* of this work:

- Modeling the transmission, propagation, and reception of CoV-2 inside the respiratory tract as an end-to-end MC system;
- Analyzing the communication-theoretic channel parameters for the end-to-end MC system model and evaluating its performance;
- Analyzing and comparing the channel parameters on the virus signal transmission for normal & asthmatic subjects.

II. RELATED WORKS

In this section, we discuss the related works involving the modeling of CoV-2 transmission, the strategies to treat CoV-2 apart from vaccines, and the progress in MC-based solutions.

A. Mathematical Modeling of COVID-19

The majority of the works on mathematical modeling of COVID-19 investigate the epidemiological development of the infection. The SIR (Susceptible, Infected, and Recovered) model forms the basis of these works. These models generate country-specific or worldwide quantitative information about the transmission of CoV-2 infection [7], [8]. There are fewer works concerning within-host modeling of CoV-2 that primarily provide deeper insights into the CoV-2 pathogenesis. The information from such mathematical approaches is essential for developing vaccines, antiviral therapies, drugs, or other therapeutic interventions [9], [10]. It is also revealed that blocking the production of progeny viruses is more effective than promoting cytotoxicity [11].

B. Alternative Therapeutic Strategies

The anticipated limited efficacy of vaccines has resulted in developing alternative therapeutic strategies, which are supposed to be potential treatments for COVID-19 infection. One of such prospects in treating COVID-19 is slowing down the outset of adaptive immunity and restraining adaptive immunity interference with innate immunity [12]. Since the severe CoV-2 infection results in a cytokine storm, the artificial liver blood purification systems serving as anti-cytokine storm targeted therapy [13] are investigated to be a potential treatment for critical patients. On the other hand, the combination of antiviral agents and immunomodulatory agents to minimize the cytokine storm is seen as a significant therapeutic strategy [14]. Moreover, a significant amount of research efforts investigates the efficacy of using Mesenchymal Stem Cells (MSC) therapy [15], monoclonal antibody therapy [16], and convalescent plasma therapy [17] as novel therapeutics.

C. Molecular Communication-based solutions

For the last decades, extensive ongoing research has resulted in the design of in vivo MC systems-based therapeutics. MC-based systems have been explored in the development of in vivo monitoring or diagnosing anomalies [18]. The use of such MC-based systems in identifying the harmful micro-organisms and achieving an ideal delivery rate of information to the targeted location [19] is seen as promising. The triggering of the immune response with molecular transmissions is also proposed as a potential treatment against severe diseases [20]. Recently, modeling virus transmission using the MC theory has been proposed by authors [21], [22], where they analyzed the detection of virus inside the human body. While, Khalid *et al.* [23] discussed the two-way communication of the virus particles to and from humans via inhalation and exhalation.

Several works [24], [25], [26], and [27] focus on the deposition of the particles in the human respiratory tract. Hofmann showed that the airflow and particle deposition are strongly correlated [24]. The transportation and deposition patterns of aerosol in the respiratory airway during a complete breathing cycle is investigated in [25]. The authors provided a stochastic model to study the distribution, deposition, and variability of aerosols in bifurcations and different alveoli

segments along the respiratory airway [26], [27]. In [28], authors discussed a Markov chain model for person-to-person transport of contaminants indoors. Kolanjiyil *et al.* showed that the size of the particles and breathing conditions influence the deposition of particles in the alveolar region [29].
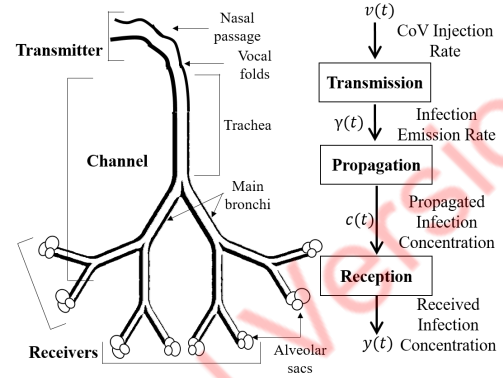

Fig. 1: MC system for virus signal pathway into the channel.

III. MAPPING OF COVID-19 PATHOGENESIS TO MOLECULAR COMMUNICATION SYSTEM

According to WHO, COVID-19 is primarily transmitted from an infected person to a healthy person through the respiratory droplets via coughing or sneezing [30]. Upon inhaling, CoV-2 attach themselves to the cellular lining of the nasal passage, get absorbed inside the host cells to replicate into progeny virus particles. The inhaled CoV-2 and progeny CoV-2 particles are transmitted through the respiratory tract to alveoli, which are tiny air sacs connected to the end branches of the central respiratory tract. After binding with CoV-2, the host cells become infected, resulting in apoptosis leading to their removal. We identify four major communication elements– transmitter, signal, channel, and receiver– involved in virus transmission from the nasal passage to the alveolar sacs, as shown in Fig. 1. The elements are as follows:

- Transmitter: The transmitter represents the nasal passage.
- Signal: The varying concentration of virus particles is represented as the signal.
- Channel: The lower respiratory tract or lower airway, including the lower part of the larynx, trachea, bronchi, and alveolar ducts, is denoted as the channel.
- Receiver: The receiver represents the epithelial and goblet cells along with the Angiotensin-Converting Enzyme 2 (ACE-2) surface receptors residing in the channel as well as alveolar sacs.

The three main processes that underline the communication mechanism of the virus particles inside the human body are 1) transmission, 2) propagation, and 3) reception. The virus signal is transmitted through the respiratory tract, which is considered as an elongated tube with a bifurcation giving rise to two main branches, as shown in Fig. 1. The tracheobronchial tree is modeled as the channel along which the virus particles propagate and are transported towards the receivers by the airflow during respiration. The production and propagation of virus signal concentration are guided by the intracellular and

the extracellular channel dynamics. The intracellular dynamics involves the entrance of the viruses into a host cell, the replication, and the release of progeny virus particles. On the other hand, the extracellular dynamics include the impact of airflow profile and diffusion. We ignore the interaction among the virus particles and consider the movements of the particles are independent of each other. The propagation of virus signal through the air-fluid medium inside the respiratory tract is assumed to follow the Brownian motion and mathematically modeled using well-known Navier-Stokes equations. The reception occurs when virus particle collides with ACE-2 receptors present in the epithelial and goblet cells along the respiratory tract.
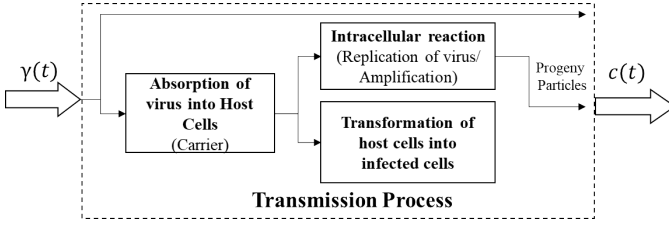

Fig. 2: Virus transmission in the MC system model.

IV. TRANSMISSION PROCESS

We model the nasal passage in the upper respiratory tract as a transmitter. On entering into the transmitter, CoV-2 particles undergo several physicochemical processes, such as *absorption*, *transformation*, and *reaction*. We draw an analogy of these processes to the working of a typical transmitter in conventional communication systems, as shown in Fig. 2. The epithelial cells in the nasal passage serve as host cells for the virus particles inside the transmitter. If the virus binds to the ACE-2 protein common in the surface of cells in the respiratory system, the susceptible host cell successfully absorbs the particle. The successful attachment of the virus particles with the host cells triggers cellular processes, such as membrane fusion, RNA release, and transcription, and chemical reactions, following which the viruses multiply rapidly. This phenomenon of replication of the virus is referred to as amplification of signal commonly observed in the communication system. The virus and progeny virus particles get transmitted into the lower respiratory tract. We consider that the number of host cells in the transmitter follows a Gaussian distribution. Furthermore, we consider that the average number of the host cells is high, and the standard deviation of the host cells is substantially lower than the average value of the host cells. Therefore, the probability of getting a non-negative value for the number of host cells is almost zero. Thus, the concentration of uninfected host cells $o(t)$ can be written as follows:

$$o(t) = \frac{1}{\sigma_o \sqrt{2\pi}} exp\left(\frac{-t^2}{2\sigma_o^2}\right), \tag{1}$$

where σ_o is the standard deviation of the distribution. The dynamics of the total number of CoV-2 $v^*(t)$ inside the

transmitter and the number of infected cells $i(t)$ are modeled as [11]:

$$\frac{di}{dt} = \beta o(t)v(t) - d_i i(t), \quad \frac{dv^*}{dt} = \wp i(t) - d_c v^*(t), \tag{2}$$

where β is constant absorption (or, binding) rate, with which the CoV-2 $v(t)$ bind and enter into the host cells, $\wp$ is the constant reaction rate inside the infected cells, with which progeny virus are produced, d_i is the death rate of infected cells, and d_c is the death rate of CoV-2. From [11], considering a quasi-steady state assumption, the number of infected cells $i(t)$ and virus particles $v(t)$ can be written as follows:

$$i(t) = \frac{d_c}{\wp}v^*(t), \quad v(t) = \frac{d_i i(t)}{\beta o(t)}. \tag{3}$$

We consider that the virus particles are amplified to $v^*(t)$. Thus substituting Eq. 3 into Eq. 2, we obtain:

$$v^*(t) = v_0 exp\left(\frac{\wp\beta}{2d_c}\left(1 + erf\left(\frac{t}{\sigma_o\sqrt{2}}\right)\right) - d_i t\right), \tag{4}$$

where v_0 is the constant amount of virus particles inhaled at time $t = 0$. Consequently, the transmitted signal is represented by the virus emission rate $\gamma(t)$, which is influenced by the production rate of progeny virus particles $\wp$ from the infected cells and is obtained as:

$$\gamma(t) = \wp i(t). \tag{5}$$

The transfer function of the transmission process $H_t(f)$ is obtained as follows:

$$H_t(f) = \frac{\Upsilon(f)}{V(f)} = \frac{\wp\beta}{d_i}exp(-2\pi^2\sigma_o^2 f^2), \tag{6}$$

where $\Upsilon(f)$ and $V(f)$ are the fourier transforms of the transmitted signal and virus signal, respectively.
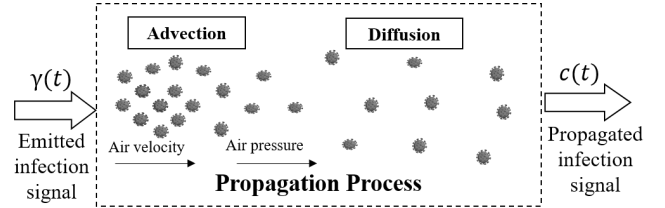

Fig. 3: Virus propagation in the MC system model.

V. PROPAGATION PROCESS

The inhaled viruses, along with newly generated viruses, are emitted from the transmitter and propagate through the airway channel under the influence of two physicochemical processes, *advection* and *diffusion*, as shown in Fig. 3. The propagation of the emitted virus signal is guided partly by the air velocity and pressure inside the channel, known as advection, partly by the Brownian motion in the channel, known as diffusion. We assume no air leakage in the channel and a consistent air pressure gradient along the channel. The effect of turbulence due to the instability in airflow is incorporated in the channel model. The emitted signal generates a concentration profile with the direction of airflow, and we considered direction
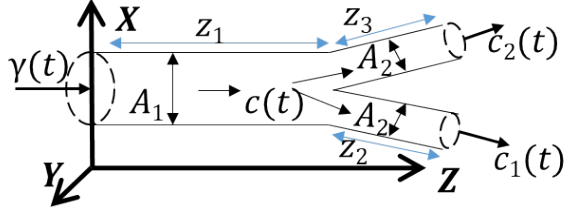
Fig. 4: A schematic diagram of the respiratory tract.

is in the z-axis, as shown in Fig. 4. By considering the geometry expanding with $x \in (-\infty, \infty)$, $y \in (-\infty, \infty)$, and $z \in [0, \infty)$, the distribution for virus concentration $c(x, y, z; t)$ in the channel is subjected to the influence of air velocity $u(x, y, z; t)$, air pressure P, air density ρ, and the dynamic viscosity of the air η. Assuming the air inside the respiratory tract to be homogeneous, incompressible, and Newtonian, the concentration of virus signal at a position (x, y, z) and time t is obtained from the solution to the Navier-Stokes equation. By considering the virus emission rate as an instantaneous impulse source $\gamma(x, y, z; t)$, the concentration of virus signal in the channel is given as [31],

$$
\frac{\partial c(x, y, z; t)}{\partial t} + \nabla(uc) - \nabla\left[\left(D + \frac{\eta_\sigma}{\sigma}\right)\nabla c\right] \\
= \gamma(x, y, z; t) = \gamma_0 \delta(x, y, z)\delta(t),
$$
(7)

where D is the particle diffusion coefficient, σ is the turbulence coefficient, η_σ is the turbulent viscosity, γ_0 is the virus signal emitted into the channel for propagation. Since the absorption of virus particles occurs on the inner surface of the respiratory tract, the boundary conditions can be written by considering the mathematical properties of absorbing receivers [32], as given below:

$$
\begin{aligned}
&c(\pm\infty, y, z; t) = 0, \quad c(x, \pm\infty, z; t) = 0, \\
&c(x, y, 0; t) = 0, \quad \frac{\partial c(x, y, \infty; t)}{\partial z} = 0, \\
&c(x, y, z, 0) = \gamma_0, \quad \frac{\partial c(x, y, z; \infty)}{\partial t} = 0.
\end{aligned}
$$
(8)

At this juncture, it is to be noted that the expressions for the concentration profile of the diffusive particles in an unbounded medium are well known. However, due to the existence of multiple processes in regard to CoV-2, such as the unique response of immune system, and the unique channel characteristics involving tidal pressure and velocity of air inside the channel, the computation of the analytical expressions for the concentration profile is not straightforward. The gradient term $\nabla(uc)$ in Eq. 7 signifies the advection process, representing the signal propagation due to air velocity. The air velocity is expressed as [33],

$$
\rho A \frac{\partial u(x, y, z; t)}{\partial t} + \rho(u.\nabla u) = \eta \nabla^2 u - A\nabla P,
$$
(9)

where A is the cross-section area of the channel. On the other hand, we consider that at the inlet as well as the entrance into the airway channel, the air velocity and gauge pressure are uniform, denoted as u_{in} and P_{in}, respectively. We define the boundary conditions at the channel bifurcation sites bifurcating

into two bronchi as shown in Fig. 4, by considering the law of flow conservation. The gauge pressure relative to atmospheric pressure across the bifurcation point remains continuous, such that $P_{z_1}(z_1) = P_{z_2}(0) = P_{z_3}(0)$. The coordinates, z_1, z_2, and z_3 represent the length of the respective branches, as depicted in Fig. 4. Likewise, the air velocity across the bifurcation remains continuous, such that $u_{z_1}(z_1) = u_{z_2}(0) = u_{z_3}(0)$. It is to be noted that at the bifurcations there is no leakage of concentration of virus signal. It follows that the signal concentration divides equally into both the branches, such that $c(t) = c_1(t) + c_2(t)$, where $c_1(t) = c_2(t)$. We consider the no-slip boundary conditions along the channel wall, given as $u(\pm\infty, y, z; t) = 0$, $u(x, \pm\infty, z; t) = 0$, $P(\pm\infty, y, z; t) = 0$, $P(x, \pm\infty, z; t) = 0$, and zero gradient velocity and pressure conditions at the entrance to the alveoli, given as $\nabla u(x, y, \infty; t) = 0$, $\nabla P(x, y, \infty; t) = 0$. Since the air velocity is large along the z-axis, the impact of advection process on the propagation of the virus signal outweigh the impact of diffusion. Thus, we reformulate the governing equation for virus signal concentration given as:

$$
\frac{\partial c}{\partial t} + u\frac{\partial c}{\partial z} - D^*\frac{\partial^2 c}{\partial x^2} - D^*\frac{\partial^2 c}{\partial y^2} = 0.
$$
(10)

where $D^* = D + \frac{\eta_\sigma}{\sigma}$, and the initial conditions are modified as $c(0, y, z; t) = \delta(y)\delta(z)\delta(t)$, $c(x, 0, z; t) = \delta(x)\delta(z)\delta(t)$, and $c(x, y, -\infty; t) = \delta(x)\delta(y)\delta(t)$. To obtain an analytical solution for the Eq. 10, we consider the method of variables separation and $c(x, y, z; t)$ can be expressed as follows:

$$
c(x, y, z; t) = X(z, x)Y(z, y)T(z, t).
$$
(11)

Substituting Eq. 11 in Eq. 10 and with further simplification, we obtain the equations given as follows:

$$
u\frac{\partial X(z, x)}{\partial z} = D^*\frac{\partial^2 X(z, x)}{\partial x^2}, \ u\frac{\partial Y(z, y)}{\partial z} = D^*\frac{\partial^2 Y(z, y)}{\partial y^2}, \\
u\frac{\partial T(z, t)}{\partial z} = -\frac{\partial T(z, t)}{\partial t},
$$
(12)

with $X(0, x) = \delta(x)$, $\left.\frac{\partial X(z, x)}{\partial z}\right|_{z\to\infty} = 0$, and $X(z, \pm\infty) = 0$; $Y(0, y) = \delta(y)$, $\left.\frac{\partial Y(z, y)}{\partial z}\right|_{z\to\infty} = 0$, and $Y(z, \pm\infty) = 0$; and $T(0, t) = \delta(t)$, $T(\infty, t) = 0$, $T(z, 0) = \gamma_0$, and $\left.\frac{\partial T(z, t)}{\partial t}\right|_{t\to\infty} = 0$. The above equations are solved by applying the Laplace transform method and are obtained as follows:

$$
X(z, x) = \sqrt{\frac{u}{\pi D^* z}}exp\left(\frac{-ux^2}{4D^* z}\right), Y(z, y) = \sqrt{\frac{u}{\pi D^* z}}exp\left(\frac{-uy^2}{4D^* z}\right), \\
T(z, t) = \gamma_0 \mathcal{U}(z - ut) + u\delta(z - ut).
$$
(13)

The analytical solution to the concentration profile of virus signal $c(x, y, z; t)$ is obtained as follows:

$$
c(x, y, z; t) = X(z, x)Y(z, y)T(z, t) \\
= \frac{u(\gamma_0 \mathcal{U}(z - ut) + u\delta(z - ut))}{\pi D^* z}exp\left(\frac{-u(x^2 + y^2)}{4D^* z}\right),
$$
(14)

where u is the average airflow speed along the respiratory tract. Since the emission rate is considered as an instantaneous im-

pulse source, the transfer function of the propagation process is obtained from taking the Fourier transform of $c(x, y, z, t)$:

$$H_p(f) = \mathscr{F}\{c(x, y, z, t)\} = C(x, y, z, f)$$

$$= C' e^{\frac{-jz}{u} 2\pi f} \left[\frac{\gamma_0}{u} \left(\pi \delta \left(\frac{-2\pi f}{u} \right) - \frac{u}{j2\pi f} \right) + \delta \left(\frac{-2\pi f}{u} \right) \right], \quad (15)$$

where $C' = \frac{u}{\pi D^* z} e^{\frac{-u(x^2+y^2)}{4D^* z}}$.

Effect of immune system: During propagation, the CoV-2 particles bind with the epithelial cells in the airway channel. The nearby host cells detect the presence of viruses from pattern recognition receptors (PPR) and secrete various signaling molecules, such as interferons, cytokines, and chemokines, to regulate immune response [34]. We choose to model the immune system's defensive behavior towards the rise of the virus as the source of attenuation encountered by the virus signal. The characteristics of the attenuation are obtained from the predator-prey system. Considering the virus particles $c(x, y, z, t)$ as the population density of the prey and the immune signaling molecules $r(x, y, z, t)$ as the population density of the predator, we model the dynamics of the immune response to the transmission of virus particles through the respiratory tract as governed by the following equations [9]:

$$\frac{\partial c}{\partial t} = D_c \nabla^2 c - \sigma \nabla c + g_c c \left(1 - \frac{c}{K} \right) - \varphi c r - d_c c, \quad (16)$$

$$\frac{\partial r}{\partial t} = D_r \nabla^2 r - \sigma \nabla r + g_r r \left(\frac{c^2}{c^2 + k_r^2} \right) - d_r r, \quad (17)$$

where D_c and D_r represent the diffusion coefficients for harmful particles and immune cells, respectively. The terms $\sigma \nabla c$ and $\sigma \nabla r$ denote the irregular migration of the harmful particles and immune cells due to the effect of turbulence, respectively. The parameters g_c, K, φ, and d_c represent the growth rate of harmful particles in the presence of immune cells, carrying capacity of the channel, predation rate on the harmful particles, and death rate of the harmful particles, respectively. We assume a logistic function for the growth of harmful particles and a log-sigmoid function of width 2 for the activation of immune cells. The immune cells are released at a rate of g_r with a half-saturation constant k_r and die at a rate of d_r. To solve the Eqs. 16 and 17 we consider the following boundary conditions:

$$c(x, y, z, 0) = \gamma_0, \qquad r(x, y, z, 0) = r_0,$$

$$\left. \frac{\partial c(x, y, z, t)}{\partial t} \right|_{t \to \infty} = \gamma_t, \qquad \left. \frac{\partial r(x, y, z, t)}{\partial t} \right|_{t \to \infty} = r_t, \quad (18)$$

where γ_0 and r_0 represent the initial amount of harmful particles and immune cells, respectively. At the time, t, γ_t and r_t are the amount of virus particles and immune cells, respectively. In order to obtain an exact analytical solution, we consider redefining the following new set of variables:

$$D_c = D_r = D, \quad \tilde{t} = \frac{t}{K}, \quad \tilde{c} = g_c c, \quad \tilde{r} = g_r r,$$

$$\tilde{x} = x \sqrt{\frac{g_c}{D_c}}, \quad \tilde{y} = y \sqrt{\frac{g_c}{D_c}}, \quad \tilde{z} = z \sqrt{\frac{g_c}{D_c}}, \quad (19)$$

and the parameters accordingly:

$$g_c K = 1, \ \sigma = \sqrt{g_c D}, \ g_c = \frac{1}{g_r}, \ g_r^2 = 1, \ g_c^2 k_r^2 = 1. \quad (20)$$

Substituting the Eqs. 19 and 20, we obtain the non-dimensional form of the Eqs. 16 and 17 as follows:

$$\tilde{c}_t = \nabla^2 \tilde{c} - \nabla \tilde{c} + \tilde{c}(1 - \tilde{c} - d_c) - \varphi \tilde{c} \tilde{r}, \quad (21)$$

$$\tilde{r}_t = \nabla^2 \tilde{r} - \nabla \tilde{r} + \tilde{r} \left(\frac{\tilde{c}^2}{1 + \tilde{c}^2} \right) - d_r \tilde{r}. \quad (22)$$

In order to keep the number of notations as minimum as practical, in the rest of the paper we omit the tilde from $\tilde{c}_t$, $\tilde{r}_t$, $\tilde{c}$, and $\tilde{r}$. It is to be noted that the immune system acting as an attenuator suppresses the propagation of the virus particles along the direction of airflow, *i.e.*, in the direction of the z-axis. The expressions for the attenuation are obtained by solving the spatio-temporal dynamics of the immune signal in the z-direction. From [35], we employ the following variables:

$$c(z, t) = \mu \frac{m_z}{m + n + e}, \quad r(z, t) = \Gamma \frac{n_z}{m + n + e}, \quad (23)$$

where m_z and n_z are the new variables, μ and Γ are the parameters and e is a constant. From [35], we get the exact solution as follows:

$$c(z, t) = \frac{v_0 \bar{c} (exp(\lambda_1 \xi) + exp(\lambda_2 \xi))}{1 + exp(\lambda_1 \xi) + exp(\lambda_2 \xi)},$$

$$r(z, t) = \frac{r_0 \bar{r} (exp(\lambda_1 \xi) + exp(\lambda_2 \xi))}{1 + exp(\lambda_1 \xi) + exp(\lambda_2 \xi)}, \quad (24)$$

where v_0 and r_0 represent the initial concentration of virus particles and immune cells, respectively, whereas, $\xi = z - ut$, and u is the velocity of air in which the waves propagates in the z-direction. The steady-state solutions are given as follows:

$$\bar{c} = \sqrt{\frac{d_r}{1 - d_r}}, \quad \bar{r} = \frac{1 - d_c - \sqrt{\frac{d_r}{1 - d_r}}}{\varphi}, \quad (25)$$

where $\lambda_{1,2}$ denotes the eigen-values, computed as $\lambda_{1,2} = -\frac{Q}{2} \pm \sqrt{\frac{Q^2 - 4R}{4}}$, and $Q = \frac{\mu - \varphi \Gamma}{\mu \Gamma (1 + \varphi)}$ and $R = 2\mu \left(1 + \frac{1}{\varphi} \right) \left(\frac{1 + \varphi - d_r}{2(\varphi - 1)} \right) + \frac{\mu(1 - d_r)}{\varphi} - \mu$.
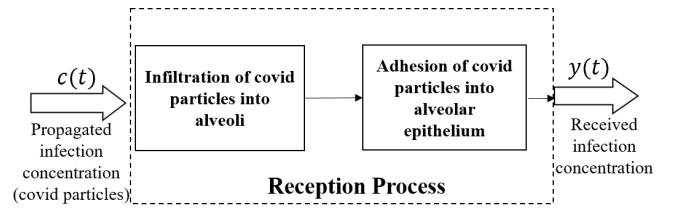

Fig. 5: Virus reception in the MC system model.

VI. RECEPTION PROCESS

The CoV-2 particles are received at a rate of $y(t)$ by the alveolar epithelium as they get transported via the advection process towards the end of the bronchi, as shown in Fig. 5. The reception of the virus signal occurring in the alveoli involves three mechanisms, such as diffusion, adhesion, and advection. As the bronchi repeatedly branch out, ending in several alveoli, the virus's movement due to advection slows down during the inspiration, leading to the rise of the diffusive movement of the virus into the alveoli. During expiration, the

advection takes over, and the signal is transported out of the alveoli. Let the concentration of virus signal inside the receiver (alveoli) be c_e. According to the law of conservation of mass, the transport of virus signal in the alveoli during the breathing cycle (inspiration and expiration), expressed as follows:

$$V\frac{dc_e}{dt} = -AD_r\frac{dc}{dz} - uAc_e + \beta c_e, \tag{26}$$

where V is the volume of the receiver (alveoli), A is the cross-sectional area of the channel, D_r is the diffusion in the receiver, c is the concentration of virus signal entering into the receiver, u is the air velocity, and β is the absorption rate at which particles are attached to the host alveolar epithelial cells. The first term represents the concentration of virus signal entering into the receivers due to the diffusion. The second term represents the concentration exit due to advection from the receiver into the channel. The last term represents the chemical reaction due to the adhesion of harmful particles to the alveolar epithelial cells. Thus, by applying the method of variables separation, the analytical solution to the concentration of the virus signal at the receiver is given by:

$$c_e(t) = \frac{-AD_r u e^{(\frac{-a}{z})}}{\pi V D z^2}\left[\left(\frac{1 - e^{(-bt-\frac{bz}{u^2})}}{b}\right)\left(\frac{a\gamma_0}{z} - \gamma_0\right) + e^{(\frac{-a}{z})}\left(1 - az - \frac{\gamma_0 z}{u}\right) + uze^{-bt}\right], \tag{27}$$

where $a = \frac{u(x^2+y^2)}{4D}$, $b = \frac{uA-\beta}{V}$, and D is the diffusion coefficient of harmful particles in the channel. Thus, the reception rate of virus particles, denoted as, $y(t)$, at the targeted sites, is defined as the concentration of harmful particles adhering to the alveolar epithelium, is expressed as follows:

$$y(t) = \frac{\beta}{V}a_e c_e(t), \tag{28}$$

where a_e is the concentration of alveolar epithelium, which is assumed to follow a Gaussian distribution. The reception process Transfer function $H_r(f)$ is computed as follows:

$$H_r(f) = \frac{Y(f)}{C(f)}, \tag{29}$$

where $Y(f)$ is obtained as:

$$Y(f) = Y'\left[\left(\frac{a\gamma_0}{z} - \gamma_0\right)\left(\frac{2\pi}{b}\delta(2\pi f) - \frac{2e^{(-\frac{bz}{u^2})}}{b^2 + (2\pi f)^2}\right) + \left(1 - az - \frac{\gamma_0 z}{u}\right)\left(\frac{2be^{(-\frac{bz}{u^2})}}{b^2 + (2\pi f)^2}\right) + uz\left(\frac{2b}{b^2 + (2\pi f)^2}\right)\right], \tag{30}$$

where $Y' = \frac{-AD_r u\beta a_e e^{(\frac{-a}{z})}}{\pi D V^2 z^2}$, while $C(f)$ is obtained from Eq. 15. The parameters $Y(f)$ and $C(f)$ are the Fourier transforms of the received virus signal and adhesive virus signal, respectively. The end-to-end Transfer function of the communication channel $H_{v,y}(f)$ is computed as follows:

$$H_{v,y}(f) = H_t(f)H_p(f)H_r(f), \tag{31}$$

where $H_t(f)$, $H_p(f)$, and $H_r(f)$ are the transfer function of the transmission process, propagation process, and reception process, respectively.

A. Distributed Receiver Scenario

The upper respiratory tract, trachea, as well as bronchi, have epithelial cells and goblet cells, which allow binding of CoV-2 particles [36]. Hence, we consider multiple receivers, say n number of receivers, are distributed along the channel. Each receiver site is assumed to contain cells with ACE-2 receptors. The CoV-2 particles uniformly diffuse in the environment and the receivers are independent of each other in the channel. Thus, the effective reception rate denoted as, $y^{eff}(t)$, any reception site is expressed as follows:

$$y^{eff}(t) \equiv \sum_{i=1}^{n}\frac{\beta_i}{V_i}t_e^i c_e^i(t), \tag{32}$$

where β_i is the binding or absorption rate at which particles enters into the host cells at the ith receiver site, V_i is the volume of the receptor of the ith receiver site, t_e^i is the concentration of epithelial cells at the ith receiver site, c_e^i is the concentration of virus signal at the ith receiver site. The effective Transfer function $H_r^{eff}(f)$ is computed as follows:

$$H_r^{eff}(f) \equiv \frac{Y^{eff}(f)}{C(f)}, \tag{33}$$

where $Y^{eff}(f)$ and $C(f)$ are the Fourier transforms of the received and propagated virus signal, respectively.

VII. CHANNEL CHARACTERISTICS

A. Channel Path Loss

In the proposed molecular-based virus communication system, the path loss, denoted as PL, is described by the decay in the virus particles inside the epithelial lining of the tracheo-bronchial channel. It is characterized by cellular absorption loss. The cellular absorption refers to the absorption of the virus particles by the immune cells and is computed as follows:

$$PL = 20log_{10}\left(\frac{C_{tx}}{C_{rx}}\right)^{\mathcal{A}}, \tag{34}$$

where C_{tx} and C_{rx} are the transmitted and the received concentration of virus particles, respectively. The absorption coefficient, denoted as, $\mathcal{A} = -\ln\frac{Kd_r}{k_r}$, is a constant term which is dependent on the characteristics of the channel components, denoted by, K, k_r, and d_r. The parameters K, k_r, and d_r represent the channel carrying capacity, half-saturation constant of the immune cells present in the epithelial lining, and death rate of immune cells, respectively.

B. Channel End-to-end Delay

In the proposed MC-based virus communication system, the transmitter transmits the virus signal to reach the receiver. The virus signal propagates via diffusion as well as advection processes to reach the alveoli. At the time $t = 0$, v_0 amount of molecules is transmitted to the inlet of the alveoli. The arrival time of the signal T_{delay} at the receiver is obtained as follows:

$$T_{delay} = T_t + T_p + T_r, \tag{35}$$

where T_t, T_p, and T_r are the the delay for the transmission, propagation, and reception processes, which are computed

from the derivative of phase $\Phi(f)$ of the respective transfer functions as follows:

$$T = -\frac{d\Phi(f)}{df}, \quad \Phi(f) = \arctan\left(\frac{Im(H(f))}{Re(H(f))}\right). \quad (36)$$

C. Channel End-to-end Normalized Gain

The end-to-end channel normalized gain is the total magnitude of the normalized gain derived from the transfer functions of the communication system and is given as follows:

$$\mathcal{G}_{tot}(f) = \mathcal{G}_t(f) \times \mathcal{G}_p(f) \times \mathcal{G}_r(f), \quad (37)$$

where the end-to-end channel normalized gain $\mathcal{G}(f)$ for three processes, namely transmission, propagation, and reception, is computed from the magnitude of the respective transfer function, normalized by its maximum value given as follows:

$$\mathcal{G}(f) = \frac{|H(f)|}{max(|H(f)|)}. \quad (38)$$

TABLE I: Simulation Parameters

Parameter	Value
Air velocity in the channel	$2.5\,m/s$
Air pressure in the channel	$16.48\,Pa$
Air density in the channel (ρ)	$1.225\,kg/m^3$
Dynamic viscosity of air (η)	$1.7894e{-}5\,kg/ms$
Turbulence coefficient (σ)	0.9
Turbulent viscosity (η_σ)	$0.36\,cm^2/s$
Initial virus concentration (v_0)	$1.18e6\,mol/cm^3$
Growth rate of virus (g_c)	$1.62\,s^{-1}$
Absorption rate of virus (β)	$3.97\,s^{-1}$
Carrying capacity of the channel (K)	$6.65e8\,mol/cm^3$
Predation rate on virus (φ)	$4.88e{-}8\,s^{-1}$
Release rate of immune cells (g_r)	$0.96\,s^{-1}$
Half-saturation constant of immune cells (k_r)	$8.58e4$
Constant release rate of virus (p)	$3.16\,s^{-1}$
Death rate of virus (d_c)	$0.6\,s^{-1}$
Death rate of infected cells (d_i)	$4.71\,s^{-1}$
Death rate of immune cells (d_r)	$2.9e{-}2\,s^{-1}$

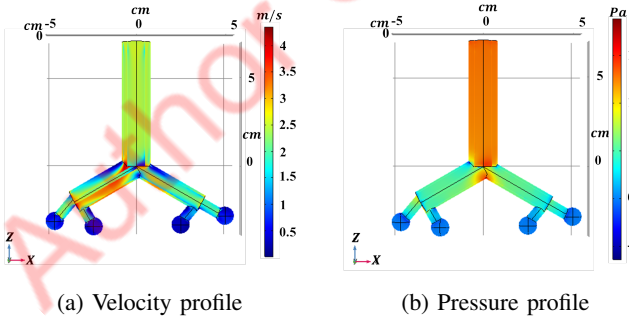(a) Velocity profile   (b) Pressure profile

Fig. 6: The airflow profile along the respiratory tract.

VIII. NUMERICAL RESULTS

We performed multiphysics-based simulations using a $3D$ geometry representing the respiratory tract to model CoV-2 MC system on COMSOL with a total simulation duration
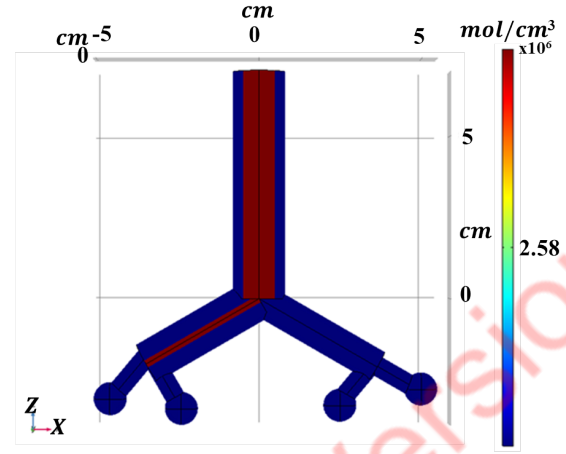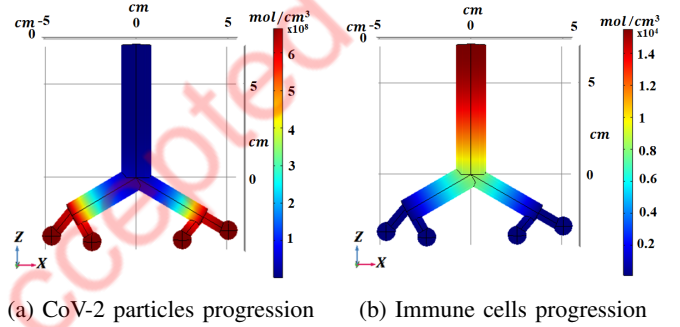

Fig. 7: Propagation of the virus signal in the channel.

(a) CoV-2 particles progression   (b) Immune cells progression

Fig. 8: Reception of the virus signal in the channel.

of $T_{sim} = 2s$ and a time step of $0.001s$. The finite-element simulations were performed in order to observe the behavior of the propagating virus along the channel for 4 to 6 hours. In the simulations, we consider the 3-D Navier–Stokes-based advection-diffusion equations in the time-varying airflow channel. The finite-element simulation environment included the dynamics of several physical phenomena, such as air velocity, air density, air pressure, and viscosity, which govern the transport of CoV-2 particles. The data involving growth rate, absorption rate, carrying capacity of the channel are considered from the existing models [9], [11], which are based on experimental data. The values against the parameters used in the simulation, which are collected from the existing literature [9], [11], [37] are listed in Table I. The characterization of airflow along the bifurcating channel provides insight into its influence on the CoV-2 propagation. The laminar flow profile for the channel commencing from the inlet of the trachea to the alveoli outlets is shown in Fig. 6. We observe that the turbulence has little impact on the transmission of the virus signal. The airflow velocity at the bifurcation increases for a brief period and gradually slows down into the alveoli, as shown in Fig. 6a. Similarly, we observe pressure drop at both the bifurcating branches, with a sharp drop between the upper inlet and the terminal outlet. The negative pressure in Fig. 6b depicts that the airflow is directed up towards the trachea from the terminal alveoli.

Fig. 7 shows the propagation of the signal concentrated towards the center of the channel under the influence of velocity
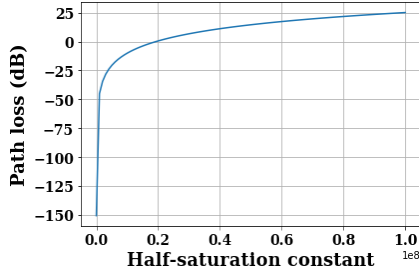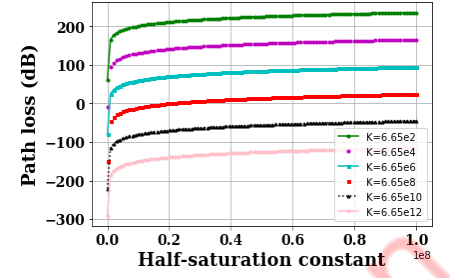
(a) Path loss vs half-saturation constant
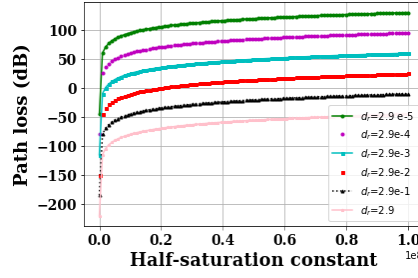
(b) Impact of immune cells death rate

(c) Impact of channel carrying capacity
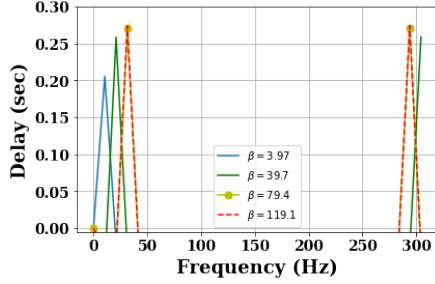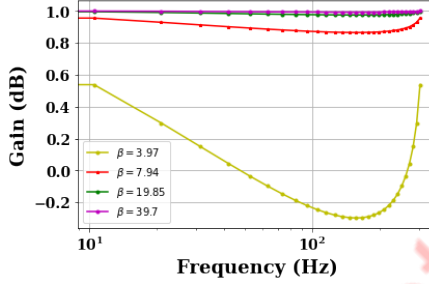
Fig. 9: End-to-end channel path loss.

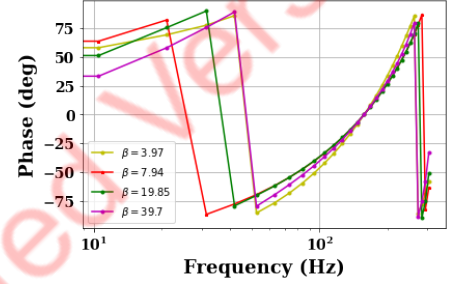Fig. 10: Channel delay variation.

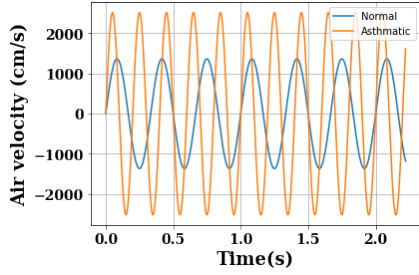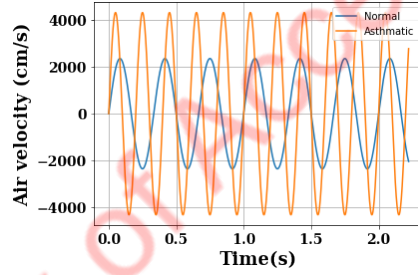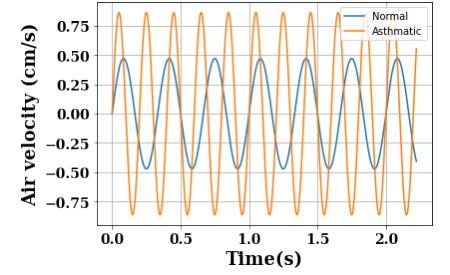Fig. 11: Channel gain variation.

Fig. 12: Channel phase variation.
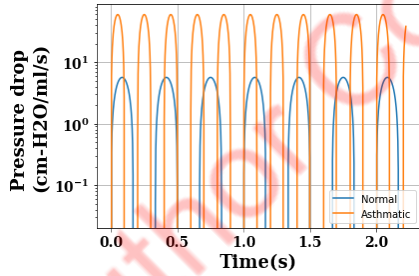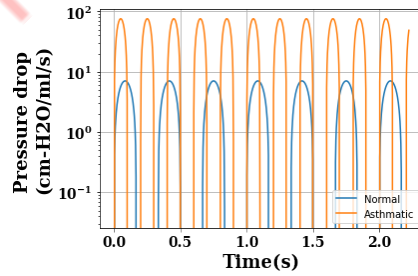

(a) At the inlet

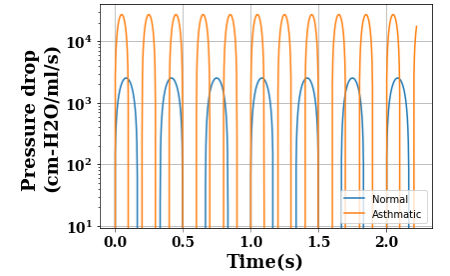(b) Through the channel

(c) At the outlet

Fig. 13: Air velocity profile through the respiratory tract for normal and asthma subjects.

(a) At the inlet

(b) Through the channel

(c) At the outlet

Fig. 14: Air pressure profile through the respiratory tract for normal and asthma subjects.

profile. The majority of the virus concentration initially flows towards the right branch at the bifurcation due to its wider diameter in the channel tree. The reception of the virus signal, as shown in Fig. 8 illustrates the trend of the progress of virus particles in Fig. 8a, as well as immune cells in Fig. 8b. The CoV-2 particles are received by the epithelial cells along the channel, which starts releasing the immune cells in response.

The signal concentration is higher towards the terminal alveoli, which are the essential target sites. With the increase in the amplitude of the virus signal, the immune response tends to increase towards the distant outlet. We performed Python-based simulations to evaluate the communication metrics.

A. Path Loss

The end-to-end channel path loss with respect to the half-saturation constant of immune cells is shown in Fig. 9. For the initial 50% of the maximum production rate of virus particles, the path loss increases more than 16 times than the remaining 50%. The half-saturation constant denotes the amount of available immune cells in the channel when half of the maximum production rate of virus particles is reached. This suggests that with the increasing value of half-saturation constant, the path loss increases, as shown in Fig. 9a. We show the effects of the varying death rate of immune cells and channel carrying capacity on the channel path loss in Figs. 9b and 9c respectively. The channel carrying capacity represents the maximum rate of virus signal transmission through the channel. We observe that the lower the death rate of immune cells, the higher path loss in the channel since it allows increase in predation of virus particles. On the other hand, with a lower channel carrying capacity, the magnitude of path loss increases.

B. Delay

The channel delay determines the amount of time taken by the virus signal to reach the receiver. In Fig. 10, we show the variation of end-to-end channel delay with the absorption rate of virus particles over frequency. We observe that for higher absorption rates, the delay in virus arrival at the receiver increases. Moreover, the delays remain constant for higher absorption rates at all the frequencies. Also, for higher absorption rates, the delays are significant at high frequencies. This response is attributed to the time taken by the virus signal to adhere to the receiver and spread.

C. Gain

The normalized gain for the end-to-end channel model is shown in Fig. 11. We observe that with the increase in frequency, the overall channel gain decreases considerably. The gradual release and the activation of immune cells result in a low gain. However, at higher frequencies, a portion of the virus signal amplifies, leading to a steep increase in gain. The higher absorption rate leads to the production of more number of progeny viruses, resulting in the maximization of the channel gain.

D. Phase

The phase for the end-to-end channel model is shown in Fig. 12, which shows a non-linear trend over frequency. The phase response remains almost constant for the different absorption rates of virus particles at higher frequencies.

IX. DISCUSSION

We discuss the effect of airflow profile on the virus signal propagation in case of asthma, a chronic respiratory disorder.

A. Air velocity

Fig. 13 illustrates the air velocity profile through the respiratory tract for both normal as well as asthmatic subjects. The velocity of air flowing into the inlet, through the channel, and at the outlet are shown in Figs. 13a, 13b, and 13c, respectively. The magnitude and direction of air velocity inside the respiratory tract change with the magnitude and direction of a respiratory cycle. From [38], the air velocity V is obtained as, $V = \frac{\pi V_t}{TA} sin\left(\frac{2\pi t}{T}\right)$, where V_t is the tidal volume, T is the breathing rate, A is the cross-sectional area of the channel, and t is time. It is common in an asthmatic patient to have a narrower respiratory tract as compared to a healthy person. The higher airflow velocities in asthmatic subjects are attributed to the lower tidal volume and respiratory rate [39], [40]. We observe that the velocity increases along the channel compared to that at the inlet. However, the velocity decreases substantially at the outlet, indicating that the rate decreases as the air reaches the alveoli.
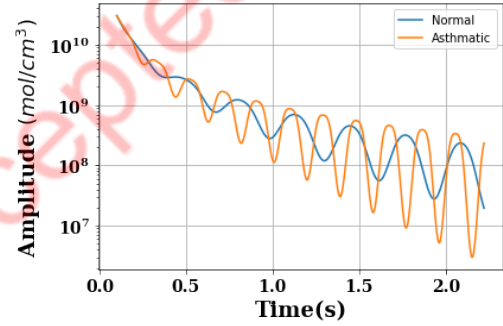

Fig. 15: Amplitude of virus signal during propagation.

B. Air pressure

The air pressure variation along the channel for both normal and asthmatic subjects during respiration is shown in Fig. 14. We calculate the air pressure drop ΔP according to the equation [39] as, $\Delta P = \frac{\pi V_t R}{T} sin\left(\frac{2\pi t}{T}\right)$, where V_t is the tidal volume, R is the resistance to airflow in the channel, T is the breathing rate, and t is time. We observe that the drop in air pressure in the channel increases for an asthmatic person. It is also evident from Figs. 14a, 14b, and 14c that the drop in pressure increases with the z-direction towards the outlets of the respiratory tract. In the case of an asthmatic person, we attribute such trend to the increased resistance to airflow along the channel. Also, the concentration of virus signal is relatively higher as shown in Fig. 15. The increment in virus signal amplitude is mainly due to the narrower cross-sectional area of the respiratory tract, where the tidal volume and breathing rate are relatively less compared to a normal person.

It is worth mentioning that the modeling exercise described in this work can be applied to model the propagation of other viruses, such as dengue and zika, inside the human body, by considering target-virus-specific unique properties (e.g., for many severe patients SARS-COV-2 often renders their immune systems overactive) into our proposed model. We also need to

consider diverse unique properties of propagation routes that virus use to spread inside the human body (e.g., dengue [41] spreads mainly via the blood circulatory system, while HIV-1 disseminates via draining lymphatics [42]).

X. CONCLUSION

In this work, we modeled the transmission of novel coronavirus inside the respiratory tract, from its entry at the nasal passage to the alveoli, using the MC theory. We take into account the geometry and characteristics of the propagation channel. Our analysis revealed that the concentration of CoV-2 signal is relatively higher at the alveoli, essentially targeting its epithelial cells, leading to the cause of Diffuse Alveolar Damage. On the other hand, there is a substantial increase of CoV-2 concentration for asthmatic patients in the respiratory system, indicating the increased risks in such subjects compared to the normal subjects. The proposed model provides us with increased knowledge about the behavior of CoV-2 propagation, which could pave the way for the development of future novel Internet of Bio-Nano Things (IoBNT)-based treatment. In the future, we plan to address the information-theoretic analysis of the proposed model. We also intend to explore the propagation of the CoV-2 particles in the vascular network.

REFERENCES

[1] J. H. University, "COVID-19 Dashboard by the Center for Systems Science and Engg. at Johns Hopkins University," Accessed 18 Jan, 2021.

[2] V. Wiwanitkit *et al.*, "SARS-CoV-2 variant: Its clinical importance and molecular epidemiology," *Journal of Medical Society*, vol. 34.

[3] K. Rajarshi, A. Chatterjee, and S. Ray, "Combating covid-19 with mesenchymal stem cell therapy," *Biotechnology Reports*, 2020.

[4] Y. Shoenfeld, "Corona (covid-19) time musings: our involvement in covid-19 pathogenesis, diagnosis, treatment and vaccine planning," *Autoimmunity Reviews*, 2020.

[5] N. Islam, S. Pal, S. Balasubramaniam, and S. Misra, "Energy-aware tracking of mobile targets by bacterial nanonetworks," *IEEE TMC*, 2020.

[6] B. D. Unluturk and I. F. Akyildiz, "An end-to-end model of plant pheromone channel for long range molecular communication," *IEEE Transactions on Nanobioscience*, vol. 16, no. 1, pp. 11–20, 2016.

[7] B. Ivorra, M. R. Ferrández, M. Vela-Pérez, and A. Ramos, "Mathematical modeling of the spread of the coronavirus disease 2019 (COVID-19) taking into account the undetected infections. the case of china," *Communications in Nonlinear Science and Numerical Simulation*, 2020.

[8] S. H. Khoshnaw, R. H. Salih, and S. Sulaimany, "Mathematical modelling for coronavirus disease (COVID-19) in predicting future behaviours and sensitivity analysis," *Mathematical Modelling of Natural Phenomena*, vol. 15, 2020.

[9] E. A. H. Vargas and J. X. Velasco-Hernandez, "In-host modelling of covid-19 kinetics in humans," *medRxiv*, 2020.

[10] C. Li, J. Xu, J. Liu, and Y. Zhou, "The within-host viral kinetics of SARS-CoV-2," *bioRxiv*, 2020.

[11] K. S. Kim, K. Ejima, Y. Ito, S. Iwanami, H. Ohashi, Y. Koizumi, Y. Asai, S. Nakaoka, K. Watashi, R. N. Thompson *et al.*, "Modelling SARS-CoV-2 Dynamics: Implications for Therapy," *medRxiv*, 2020.

[12] S. Q. Du and W. Yuan, "Mathematical modeling of interaction between innate and adaptive immune responses in COVID-19 and implications for viral pathogenesis," *Journal of Medical Virology*, 2020.

[13] Y. Zhang, L. Yu, L. Tang, M. Zhu, Y. Jin, Z. Wang, and L. Li, "A promising anti-cytokine-storm targeted therapy for COVID-19: the artificial-liver blood-purification system," *Engg. (Beijing, China)*, 2020.

[14] M. Zhao, "Cytokine storm and immunomodulatory therapy in COVID-19: role of chloroquine and anti-IL-6 monoclonal antibodies," *International Journal of Antimicrobial Agents*, 2020.

[15] G. Moll, N. Drzeniek, J. Kamhieh-Milz, S. Geissler, H.-D. Volk, and P. Reinke, "MSC therapies for COVID-19: Importance of patient coagulopathy, thromboprophylaxis, cell product quality and mode of delivery for treatment safety and efficacy," *Front. Immunol.*, 2020.

[16] B. Shanmugaraj, K. Siriwattananon, K. Wangkanont, and W. Phoolcharoen, "Perspectives on monoclonal antibody therapy as potential therapeutic intervention for Coronavirus disease-19 (COVID-19)," *APJAI*, vol. 38, no. 1, pp. 10–18, 2020.

[17] L. Chen, J. Xiong, L. Bao, and Y. Shi, "Convalescent plasma as a potential therapy for COVID-19," *The Lancet Infectious Diseases*, vol. 20, no. 4, pp. 398–400, 2020.

[18] N. Varshney, A. Patel, Y. Deng, W. Haselmayr, P. K. Varshney, and A. Nallanathan, "Abnormality detection inside blood vessels with mobile nanomachines," *IEEE TMBMC*, vol. 4, no. 3, pp. 189–194, 2018.

[19] H. K. Rudsari, N. Mokari, M. R. Javan, E. A. Jorswieck, and M. Orooji, "Drug release management for dynamic TDMA-based molecular communication," *IEEE TMBMC*, vol. 5, no. 3, pp. 233–246, 2019.

[20] L. Felicetti, M. Femminella, and G. Reali, "A simulation tool for nanoscale biological networks," *Nano Comm. Networks*, vol. 3, 2012.

[21] M. Khalid, O. Amin, S. Ahmed, and M.-S. Alouini, "System modeling of virus transmission and detection in molecular communication channels," in *IEEE ICC*, 2018, pp. 1–6.

[22] M. Khalid, O. Amin, S. Ahmed, B. Shihada, and M.-S. Alouini, "Communication through breath: Aerosol transmission," *IEEE Communications Magazine*, vol. 57, no. 2, pp. 33–39, 2019.

[23] Khalid, Maryam and Amin, Osama and Ahmed, Sajid and Shihada, Basem and Alouini, Mohamed-Slim, "Modeling of Viral Aerosol Transmission and Detection," *IEEE Transactions on Communications*, 2020.

[24] W. Hofmann, "Modelling inhaled particle deposition in the human lung—A review," *J. Aerosol Sci.*, vol. 42, no. 10, 2011.

[25] L. Koblinger and W. Hofmann, "Monte Carlo modeling of aerosol deposition in human lungs. Part I: Simulation of particle transport in a stochastic lung structure," *J. Aerosol Sci.*, vol. 21, no. 5, 1990.

[26] W. Hofmann and L. Koblinger, "Monte Carlo modeling of aerosol deposition in human lungs. Part II: Deposition fractions and their sensitivity to parameter variations," *J. Aerosol Sci.*, vol. 21, no. 5, 1990.

[27] Hofmann, Werner and Koblinger, Laszlo, "Monte Carlo modeling of aerosol deposition in human lungs. Part III: Comparison with experimental data," *J. Aerosol Sci.*, vol. 23, no. 1, 1992.

[28] C. Chen, "Modeling person-to-person contaminant transport in enclosed environments," 2015.

[29] A. V. Kolanjiyil and C. Kleinstreuer, "Modeling airflow and particle deposition in a human acinar region," *Comput Math Methods Med*, 2019.

[30] A. Africa, "Modes of transmission of virus causing covid-19: implications for IPC precaution recommendations," *WHO*, March 2020.

[31] C. Kleinstreuer and Z. Zhang, "Airflow and particle transport in the human respiratory system," *Annu. Rev. Fluid Mech.*, vol. 42, 2010.

[32] V. Jamali, A. Ahmadzadeh, W. Wicke, A. Noel, and R. Schober, "Channel modeling for diffusive molecular communication—A tutorial review," *Proceedings of the IEEE*, vol. 107, no. 7, pp. 1256–1301, 2019.

[33] E. G. Tsega, "Computational fluid dynamics modeling of respiratory airflow in tracheobronchial airways of infant, child, and adult," *Comput Math Methods Med*, 2018.

[34] A. H. Newton, A. Cardani, and T. J. Braciale, "The host immune response in respiratory virus infection: balancing virus clearance and immunopathology," in *Seminars in Immunopathology*, vol. 38, no. 4. Springer, 2016, pp. 471–482.

[35] S. Petrovskii, H. Malchow, and B.-L. Li, "An exact solution of a diffusive predator–prey system," *Proc. Math. Phys. Eng. Sci.*, vol. 461, no. 2056, pp. 1029–1053, 2005.

[36] R. J. Mason, "Pathogenesis of COVID-19 from a cell biology perspective," 2020.

[37] S. Qi, B. Zhang, Y. Teng, J. Li, Y. Yue, Y. Kang, and W. Qian, "Transient dynamics simulation of airflow in a CT-scanned human airway tree: more or fewer terminal bronchi?" *Comput Math Methods Med*, 2017.

[38] J. Elcner, F. Lizal, J. Jedelsky, and M. Jicha, "Study of airflow in the trachea of idealized model of human tracheobronchial airways during breathing cycle," in *EPJ Web of Conferences*.

[39] I. Herman, *Physics of the human body*. Springer Science & Business Media, 2007.

[40] D. R. Stather and T. E. Stewart, "Clinical review: Mechanical ventilation in severe asthma," *Critical Care*, vol. 9, no. 6, 2005.

[41] S. Pal, N. Islam, S. Misra, and S. Balasubramaniam, "In vivo channel characterization for dengue virus infection," in *Proceedings of the Sixth Annual ACM NanoCom*, 2019, pp. 1–7.

[42] L. Bracq, M. Xie, S. Benichou, and J. Bouchet, "Mechanisms for cell-to-cell transmission of HIV-1," *Frontiers in immunology*, vol. 9, 2018.

Nabiul Islam Nabiul Islam received the Ph.D. degree from the Indian Institute of Technology (IIT) Kharagpur, India, in 2016, and M.Tech in Computer Science and Engineering from University of Calcutta in 2010. He is a Marie Curie fellow, having worked at TSSG, Waterford Institute of Technology (WIT) in Ireland. He worked as an ERCIM Research Fellow on characterization of the networks of head direction neuronal cells at the Department of Electronics and Telecommunications in Norwegian University of Science and Technology (NTNU), Norway from December 2016 to December 2017. His current research interests include Molecular Communication, Terahertz wireless networks and Neuro-engineering.

Saswati Pal Saswati Pal is an Institute Research Scholar and pursuing her Ph.D. from the School of Nano-Science and Technology, Indian Institute of Technology (IIT) Kharagpur, India. Prior to that, she was working as a Senior Research Fellow with the Department of Computer Science and Engineering, Indian Institute of Technology Kharagpur, India. She received her M.Tech degree in Electronics and Communication from National Institute of Technology Jalandhar, India in 2016. The current research interests of Ms. Pal include Molecular Communication, Internet of Things, and Wireless Body Area Networks.

Sudip Misra (M'09 — SM'11) He received the Ph.D. degree in computer science from Carleton University, Ottawa, ON, Canada. He is a Professor with the Department of Computer Science and Engineering, Indian Institute of Technology (IIT) Kharagpur, India. Prior to this, he was associated with Cornell University (USA), Yale University (USA), Nortel Networks (Canada), and the Government of Ontario (Canada). He possesses several years of experience working in the academia, government, and private sectors in research, teaching, consulting, project management, architecture, software design, and product engineering roles. His current research interests include wireless ad hoc and sensor networks, Internet of Things (IoT), computer networks, learning systems, and algorithm design for emerging communication networks.